



# High-power vertical external-cavity surface-emitting laser emitting switchable wavelengths

JIYE ZHANG,<sup>1,2</sup> JIANWEI ZHANG,<sup>1,\*</sup> ZHUO ZHANG,<sup>1,2</sup> YUGANG ZENG,<sup>1</sup> XING ZHANG,<sup>1</sup> HONGBO ZHU,<sup>1</sup> YOUWEN HUANG,<sup>1</sup>  LI QIN,<sup>1</sup> YONGQIANG NING,<sup>1</sup> LIJUN WANG,<sup>1</sup> AND JINJIANG CUI<sup>3,4</sup>

<sup>1</sup>State Key Laboratory of Luminescence and Application, Changchun Institute of Optics, Fine Mechanics and Physics, Chinese Academy of Sciences, Changchun 130033, China

<sup>2</sup>Center of Materials Science and Optoelectronics Engineering, University of Chinese Academy of Sciences, Beijing 100049, China

<sup>3</sup>Suzhou Institute of Biomedical Engineering and Technology, Chinese Academy of Sciences, Suzhou 215163, China

<sup>4</sup>Jinan Guoke Medical Science & Technology Development Co., Ltd, Jinan 250101, China

\*gongchangjianwei@163.com

**Abstract:** In this paper we reported on the optically pumped VECSELs with switchable lasing wavelengths. The two lasing wavelengths of  $\lambda \approx 954$  nm and 1003 nm are generated at different pumping powers from the same gain chip. The thermal rollover of output power is observed twice, and the first rollover on the power curve indicates the switch of lasing wavelength. During the operation of our VECSEL, the increase of pumping power changes the temperature within the gain chip, and thus the gain spectrum is tuned to the one of two modes, which is defined by the dips on the reflectivity spectrum. The maximum output power of each wavelength exceeds 2.2 W at -5 °C. The dual-wavelength emission at  $\lambda \approx 954$  nm and 1003 nm is also demonstrated, and the output power of the dual-wavelength emission reached nearly 2 W.

© 2020 Optical Society of America under the terms of the [OSA Open Access Publishing Agreement](#)

## 1. Introduction

Over the past years, optically pumped vertical external cavity surface-emitting lasers (VECSELs) has been proved to be a flexible multi-wavelength emission platform with high brightness and output power [1–3]. VECSELs can be designed for a wide range of fundamental operating wavelengths from 670 nm to 2800 nm [4–6]. Also the external cavity design can provide an excellent configuration for optical elements, thus the Q-switching, mode-locking and non-linear wavelength changing can be realized [7–9]. The intrinsic advantages of the VECSEL can thus be utilized for realizing unique operational requirements such as dual wavelength sources. High brightness semiconductor lasers operating at two different wavelengths are of great interest in a range of applications, including free-space wavelength-multiplexed optical communications and intracavity nonlinear frequency mixing [10,11].

Several approaches have already been demonstrated to achieve dual-wavelength lasing until now. The mostly used approach is to apply one external cavity with different gain chips for each wavelength [12–14]. This solution is quite bulky, and always needs complex optics, such as the vertical coupled-cavity. Generally, the most preferable solution is the single chip generating dual-wavelength emission simultaneously in the same optical cavity. Morozove et al. proposed the theoretical model for such a laser [15], and then dual-wavelength emission from an optically pumped VECSEL was demonstrated [16]. The gain region of gain chip in such VECSEL system is divided into two or three sections, including the long-wavelength section and short-wavelength

section. The optical field distribution in the gain region must be carefully designed to avoid the optical absorption and interaction between the fields.

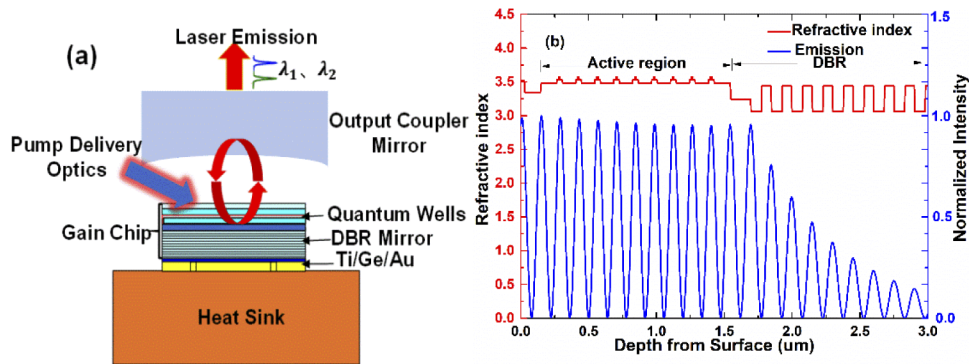
In this paper, we have developed optically pumped VECSEL with switchable emission wavelengths which are separated near 50 nm. The gain region used in our gain chip is identical. Dips on the reflectivity spectrum of our designed gain chip provide several possible emitting wavelengths. And the well-designed photoluminescence (PL) position of gain region supports the wavelength switch between two different wavelengths. The two emission wavelengths can be switched by changing the pumping power. The two wavelengths can also emit simultaneously, and the output power at dual-wavelength lasing reaches nearly 2 W. The Optical far-field intensity distribution shows smooth circle shape.

## 2. Design and fabrication

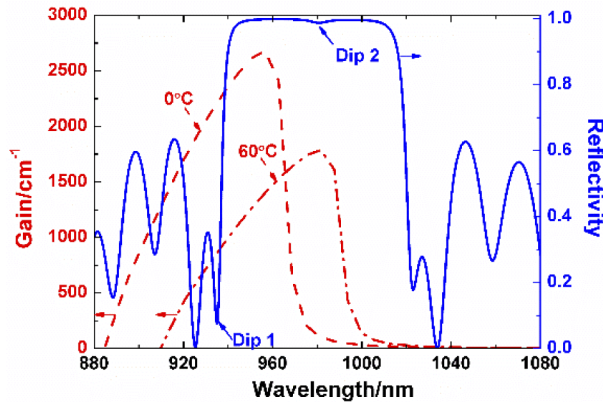
A typical “bottom emitter” VECSEL design [17] is utilized in our investigations. The active region of ten InGaAs multi-quantum wells (MQWs) is grown on an undoped GaAs substrate, and then a high reflectivity ( $R > 99.9\%$ ) distributed Bragg reflector (DBR) mirror was grown following the active region. A GaInP etch stop layer between the active region and the substrate is used to ease the chemical substrate removal [18], and then removed by second selective etch. The active region consisted of nine 8-nm InGaAs quantum wells, and each QW is surrounded by 12-nm GaAsP strain-compensated barriers. The GaAs layers are used as the pump-absorbing layers. The thickness of GaAs layers was optimized such that each quantum well is positioned at an antinode of the optical field within the gain chip. Thus, the resonant periodic gain can be achieved [19]. The DBR stack mirror is made up of 27.5 pairs of alternating GaAs/AlAs layers. In order to maximize the thermal management, the epitaxial side of the VECSEL wafer was solder bonded on a chemical vapor deposition (CVD) diamond. After the removal of the GaAs substrate, the devices are tightly fixed on a copper heat sink. The temperature of heat sink is controlled by a thermo electric cooler (TEC), and the hot side of TEC is mechanically mounted on the water-cooled heat sink.

Figure 1(a) shows the basic schematic of VECSEL cavity used in our experiment. An optical mirror with a reflectivity of 96% and a radius of curvature of 80 cm was used as the output mirror. The total length of the linear cavity is  $\approx 70$  cm. The samples were optically pumped by a fiber coupled 808 nm laser diode with a pump spot diameter of around 200  $\mu\text{m}$ . The pump beam was focused onto the VECSEL chip at an angle of  $30^\circ$  with respect to the surface normal. Figure 1(b) presents the refractive index and optical field distributions of our wavelength-switchable VECSEL. The periodic antinode of optical standing wave is designed exactly at the position of QWs. And this arrangement avoids spatial hole burning effects and leads to a wideband gain enhancement around the design wavelength Semiconductor disk lasers for the generation of visible and ultraviolet radiation [20].

For optimum performance, the gain spectrum of active region should be designed corresponding to the dip on the reflectivity band [21]. The presence of such a dip provides a wavelength selective enhancement of the gain chip. However, the gain peak of QWs shifts nearly 5 times faster than the reflectivity band of VECSEL. Thus, the gain offset is considered in our design, as shown in Fig. 2. And this gain offset can compensate the thermal detuning at higher temperatures and powers at the expense of a slight increase in threshold power. In Fig. 2, the reflectivity spectrum at  $0^\circ\text{C}$  shows that the mirror stop-band is 65 nm-broad, and the resonance marked by a reflectivity dip (dip 2) is at 978 nm. A detuning between QW gain peak and microcavity resonance reaches nearly 25 nm at  $0^\circ\text{C}$ . And the reflectivity dip near the center of stop band can hardly receive any effective gain at  $0^\circ\text{C}$ . But another reflectivity dip near the stop band (dip 1) can match the gain peak well. As the temperature of VECSEL is increased, the gain peak shifts quickly toward the reflectivity dip near the center of stop band. Thus, the gain spectrum can support another resonant wavelength at higher temperatures.



**Fig. 1.** (a) The schematic of 980-nm VECSEL device. (b) The simulated standing-wave distribution of VECSEL structure.



**Fig. 2.** Gain spectra (red dashed line) of QWs at 0 °C and 60 °C when the carrier density within QWs is  $5 \times 10^{18} \text{ cm}^{-3}$ , and the reflectivity spectrum (blue solid line) of gain chip.

### 3. Result

The designed gain chip structure was grown on the Si-doped GaAs substrate by Aixtron 200/4 MOVPE system. Side view sketch of a typical VECSEL gain chip by scanning electron microscope image (SEM) are shown in Fig. 3(a). DBR layers with high thickness uniformity are achieved. The thickness of repeated layers in the stack mirror is nearly the same as the others, thus we can get the proper constructive interference between all the layers. The active region is right next to the DBR layers. The GaInP etch stop layer can be clearly distinguished by its light color in Fig. 3(a), as the electron and hole mobility of GaInP material are rather low than that of AlGaAs materials.

A  $3 \times 3 \text{ mm}^2$  piece of the wafer was soldered on a 300  $\mu\text{m}$  thick CVD diamond. After the substrate removal, the sample is mounted on a copper holder. The measured reflectivity spectrum at 0 °C is shown in Fig. 3(b). The dip in reflectance clearly indicate the wavelength of FP resonances, which is 974 nm. Dips near the reflectance stop band indicate other wavelengths near the 930 nm. The PL spectrum unmodified by the microcavity is taken from the edge of gain chip and shown in Fig. 3(b). The PL peak is blue shifted about 25 nm with respect to the FP wavelength. Thus, the PL spectrum already matches the dips near the stop band at this temperature.

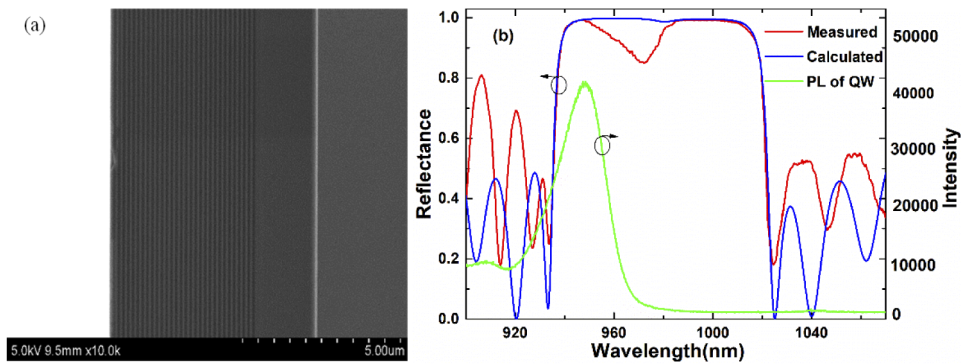


**Fig. 3.** (a) SEM image of gain chip with active region and stacked DBR mirror, the bright layer indicates GaInP etch stop layer. (b) The reflectance  $R$  and PL spectra for the gain chip at  $0\text{ }^{\circ}\text{C}$ . The PL spectrum is taken from the edge of gain chip.

The PL spectra measured from the surface and edge of gain chip are shown in Fig. 4. The PL spectrum from the surface is obviously modified by the microcavity, and peaks on this PL spectrum corresponds to the dips on the reflectance spectrum in Fig. 3(b). The two main peaks on the PL spectrum from the surface indicate emission at wavelengths near the 940 nm and 980 nm, respectively. The waveform near the 940 nm seems much wider than that near the 980 nm, and many peaks near the 940 nm appears. The much stronger emission intensity of 940 nm than that of 980 nm indicates the priority of emission at the wavelength of 940 nm. The peak on the PL spectrum from the edge of gain chip is also affected by the FP resonance. Two peaks appear on the PL spectrum, and this represents the identical parameters of periodic QWs in the active region and the FP resonance spectrum.

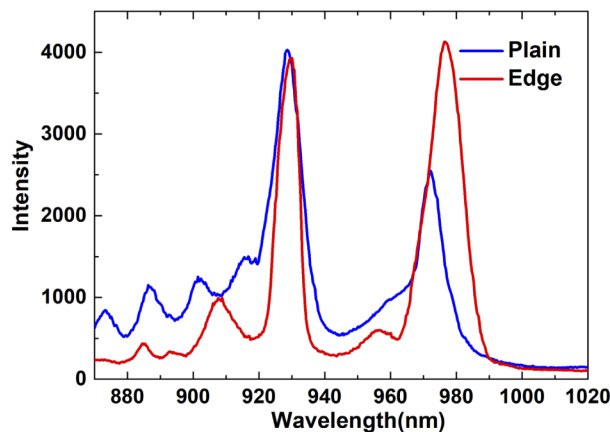


**Fig. 4.** PL spectra from the edge and surface of gain chip under the 808 nm-pumping power of 3 W.

Figure 5(a) shows the output power obtained from our device. The power curve shows two ranges of linear dependency on the pumping power. The first linear region has the threshold pumping power of 3 W. The thermal rollover would appear on the output power curve after a linearly increase with the pumping power. But the output power would increase again after the first rollover as the pumping power is further increased. The pumping power corresponding to the start point of the second linear range is called the second threshold power. The threshold power

at the first range of power curve doesn't differ too much at different operating temperatures, but the second threshold power differs with each other. As the operating temperature is decreased from 5 °C to -5 °C, the second threshold power is increased from 12 W to 17 W. And this means that the second range of power curve is related to the internal heat accumulation of gain chip. The rollover would also appear on the second range of power curve, especially for the sample operating at 5 °C. The thermal rollover power on the first linear curve can be improved from 1.2 W to 2.2 W if the operating temperature is decreased from 5 °C to -5 °C in Fig. 5(a). And the corresponding pump efficiency of the first linear curve can be improved from 0.1 to 0.15. At higher temperature of 5 °C, the second linear curve starts to rollover before reaches the maximum output power of 2.5 W. The maximum output power can reach nearly 3W when the temperature of heat sink is controlled at 0 °C and -5 °C.

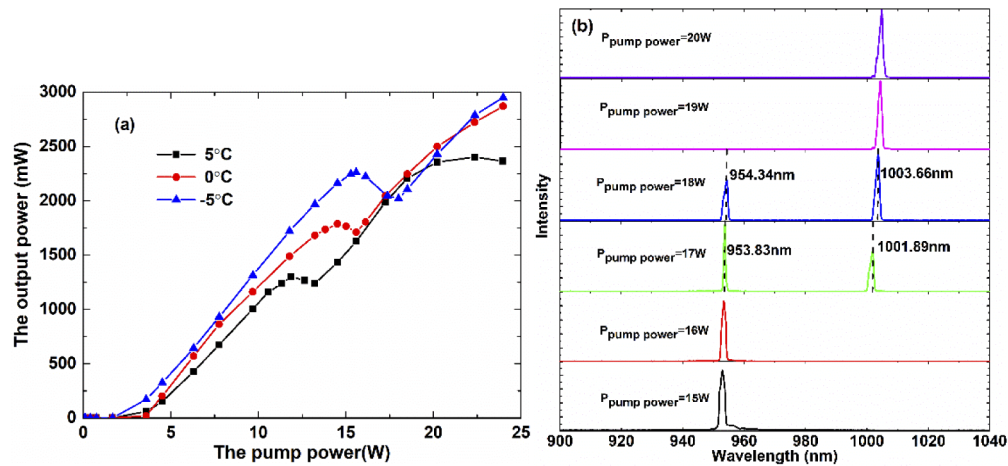
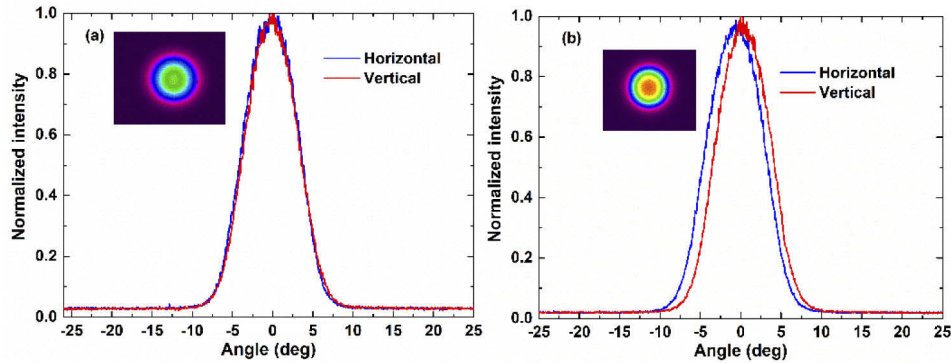


**Fig. 5.** (a) Light output power against pump power at different heat-sink temperatures when the temperature of heat sink was controlled at -5 °C, 0 °C and 5 °C. (b) the lasing wavelength changing with pump powers at -5 °C.

Figure 5(b) depicts the lasing spectra changing with pumping powers at -5 °C. Two different wavelengths of  $\lambda \approx 950$  nm and 1000 nm can be emitted from a single VECSEL device at different pumping powers. Near 50 nm-wavelength-jump can be observed when the pumping power is increased from 15 W to 18 W. And the most important is that the dual-wavelength can also be emitted simultaneously when the pumping power is around 17 W-18 W, corresponding to the pumping powers of rollover region at the first range of power curve, as shown in Fig. 5(a). The internal self-heating effect caused by the increased pumping power changes the emitting wavelength of our VECSEL device. As shown in Fig. 3(b), the large gain offset of nearly 25 nm is used in our VECSEL structure. And the wavelength of 940 nm is firstly emitted at lower pumping power, which can also be seen in Fig. 4. The temperature within the gain chip increases rapidly with increased pumping power due to the self-heating effect [22]. The gain spectrum is red shifted at higher pumping power, due to the increased temperature. Thus, the gain spectrum would deviate from 940 nm and move toward 1000 nm, then the rollover of 940 nm-emission is observed on the output power curve in Fig. 5(a). As the pumping power is further increased, the gain spectrum would be shifted to match the microcavity resonance wavelength of 1000 nm. And the wavelength switch from 940 nm to 1000 nm is realized at last.

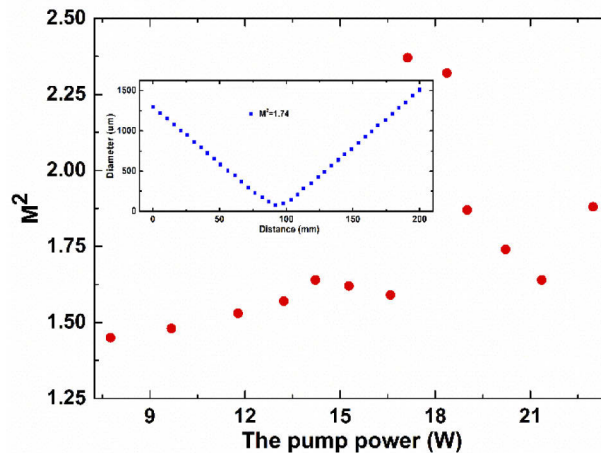
The far-fields of VECSEL device pumped at 11 W and 20 W are measured and illustrated in Fig. 6, and the emitting wavelength is 950 nm and 1000 nm at these pumping powers, respectively. Both the two far fields show Gaussian cross-sections in both dimensions. The divergence angles of full width at half maximum (FWHM) are 8.16 ° and 8.12 ° at two orthogonal directions in

Fig. 6(a), and  $8.08^\circ$  and  $7.84^\circ$  in Fig. 6(b). Although the emitting wavelength changes with the increasing pumping power, the output far field is still unchanged.



**Fig. 6.** Emission far-fields of VECSEL device under the pumping power of 11 W (a) and 20 W (b), measured at heat-sink temperature of  $-5^\circ\text{C}$ , inserted is the output beam profile captured by a CCD camera.

The beam quality  $M^2$  of the VECSEL device is measured by a commercial beam propagation analyzer M2MS-BP209. Figure 7 shows the beam quality  $M^2$  of the VECSEL device under various pump powers from 7 W to 23 W at  $-5^\circ\text{C}$ . The  $M^2$  is slightly better at the pump power below 17 W. When the pumping power is increased from 17 W to 18 W, the value of  $M^2$  is higher than 2. This is because the competition between  $\lambda \approx 950\text{ nm}$  and  $1000\text{ nm}$  emitting modes results in the poor beam quality  $M^2$ . The value of  $M^2$  drops below 2 with the further increase of pump power. The measured value of  $M^2$  is 1.74 at pump power of 20 W, as shown in the inset of Fig. 7. As the pump power continues to increase, the  $M^2$  curve shows the fluctuation, which may be resulted from the competition of high-order modes. Although the value of  $M^2$  for the VECSEL is higher under the dual-wavelength operation, the VECSEL device suffers from reduced beam quality along with power scaling on the overall trend.



**Fig. 7.** Beam quality  $M^2$  factors of the VECSEL device at  $-5^\circ\text{C}$ . The inset is the  $M^2$  measurement at the 20 W pump power.

#### 4. Conclusion

The optically pumped VECSELS device with switchable emitting wavelengths is presented. By the structure with large gain offset, the lasing wavelength of VECSEL can be switched between 954 nm and 1003 nm from a single gain chip. The dual-wavelength emission is also demonstrated under specific pumping powers. The maximum output power of each wavelength exceeds 2.2 W at -5 °C. Gaussian-shape far fields in both dimensions are gained under different pumping powers. The results we presented suggest the potential of VECSELS in WDM and generating THz wavelengths.

#### Funding

National Key Research and Development Program of China (2018YFB2002401); National Natural Science Foundation of China (11674314, 11774343, 61434005, 61727822, 61874117, 61991433); Equipment Advanced Research Fund (61404140107); Jilin Scientific and Technological Development Program (20180201119GX, 20190302042GX); Jinan Science and Technology Bureau (2019GXRC041); STS Innovation and Entrepreneurship Guidance Project of Chinese Academy of Sciences (KFJ-STIS-SCYD-318).

#### Disclosures

The authors declare no conflicts of interest.

#### References

1. B. Heinen, T. L. Wang, M. Sparenberg, A. Weber, B. Kunert, J. Hader, S. W. Koch, J. V. Moloney, M. Koch, and W. Stolz, "106 W continuous-wave output power from vertical-external-cavity surface-emitting laser," *Electron. Lett.* **48**(9), 516–517 (2012).
2. G. Y. Hou, S. L. Shu, J. Feng, A. Popp, B. Schmidt, H. Y. Lu, L. J. Wang, S. C. Tian, C. Z. Tong, and L. J. Wang, "High power (>27 W) semiconductor disk laser based on pre-metalized diamond heat-spreader," *IEEE Photonics J.* **11**(2), 1–8 (2019).
3. K. Nechay, A. Mereuta, C. Paranthoen, G. Brévalle, C. Levallois, M. Alouini, N. Chevalier, M. Perrin, G. Suruceanu, A. Caliman, E. Kapon, and M. Guina, "High-power 760 nm VECSEL based on quantum dot gain mirror," *IEEE J. Quantum Electron.* **56**(4), 1–4 (2020).
4. S. Calvez, J. E. Hastie, M. Guina, O. G. Okhotnikov, and M. D. Dawson, "Semiconductor disk lasers for the generation of visible and ultraviolet radiation," *Laser Photonics Rev.* **3**(5), 407–434 (2009).
5. A. Rahimi-Iman, "Recent advances in VECSELS," *J. Opt.* **18**(9), 093003 (2016).
6. M. Guina, A. Rantamäki, and A. Härkönen, "A. Optically pumped VECSELS: review of technology and progress," *J. Phys. D: Appl. Phys.* **50**(38), 383001 (2017).
7. B. W. Tilma, M. Mangold, C. A. Zaugg, S. M. Link, D. Waldburger, A. Klenner, A. S. Mayer, E. Gini, M. Golling, and U. Keller, "Recent advances in ultrafast semiconductor disk lasers," *Light: Sci. Appl.* **4**(7), e310 (2015).
8. E. J. Saarinen, A. Härkönen, R. Herda, S. Suomalainen, L. Orsila, T. Hakulinen, M. Guina, and O. G. Okhotnikov, "Harmonically mode-locked VECSELS for multi-GHz pulse train generation," *Opt. Express* **15**(3), 955–964 (2007).
9. L. Jiang, R. Zhu, M. Jiang, D. zhang, Y. Cui, P. Zhang, and Y. Song, "Frequency doubling of an InGaAs multiple quantum wells semiconductor disk laser," *Superlattices Microstruct.* **113**, 118–128 (2018).
10. R. Purvinskis, D. Giggenbach, H. Henniger, and N. Perlot, "Multiple-wavelength free-space laser communications," *Proc. SPIE* **4975**, 12–19 (2003).
11. M. Scheller, J. M. Yarborough, J. V. Moloney, M. Fallahi, M. Koch, and S. W. Koch, "Room temperature continuous wave milliwatt terahertz source," *Opt. Express* **18**(26), 27112–27117 (2010).
12. C. Hessenius, M. Lukowski, and M. Fallahi, "High-power tunable two-wavelength generation in a two chip co-linear T-cavity vertical external-cavity surface-emitting laser," *Appl. Phys. Lett.* **101**(12), 121110 (2012).
13. F. Zhang, M. Gaafar, C. Möller, W. Stolz, M. Koch, and A. Rahimi-Iman, "Dual-wavelength emission from a serially connected two-chip VECSEL," *IEEE Photonics Technol. Lett.* **28**(8), 927–929 (2016).
14. H. Guoyu, C. Kriso, F. Zhang, M. Wichmann, W. Stolz, K. A. Fedorova, and A. Rahimi-Iman, "Two-chip power-scalable THz-generating semiconductor disk laser," *Opt. Lett.* **44**(16), 4000–4003 (2019).
15. Y. Morozov, I. Nefedov, and V. Aleshkin, "Nonlinear frequency conversion in a double vertical-cavity surface-emitting laser," *Semiconductors* **38**(11), 1350–1355 (2004).
16. T. Leinonen, Y. A. Morozov, A. Harkonen, and M. Pessa, "Vertical external-cavity surface-emitting laser for dual-wavelength generation," *IEEE Photonics Technol. Lett.* **17**(12), 2508–2510 (2005).
17. A. C. Tropper and S. Hoogland, "Extended cavity surface-emitting semiconductor lasers," *Prog. Quantum Electron.* **30**(1), 1–43 (2006).

18. T. S. Wilhelm, C. W. Soule, M. A. Baboli, C. J. O'Connell, and P. K. Mohseni, "Fabrication of Suspended III-V Nanofoils by Inverse Metal-Assisted Chemical Etching of  $\text{In}_{0.49}\text{Ga}_{0.51}\text{P}/\text{GaAs}$  Heteroepitaxial Films," *ACS Appl. Mater. Interfaces* **10**(2), 2058–2066 (2018).
19. H. H. Park and B. S. Yoo, "Low threshold current density and high efficiency surface-emitting lasers with a periodic gain active structure," *ETRI J.* **17**(1), 1–10 (1995).
20. L. Fan, J. Hader, M. Schillgalies, M. Fallahi, A. R. Zakharian, J. V. Moloney, R. Bedford, J. T. Murray, S. W. Koch, and W. Stolz, "High-power optically pumped VECSEL using a double-well resonant periodic gain structure," *IEEE Photonics Technol. Lett.* **17**(9), 1764–1766 (2005).
21. J. Muszalski, A. Broda, A. Trajnerowicz, A. Wójcik-Jedlińska, R. P. Sarzała, M. Wasiak, P. Gutowski, I. Sankowska, J. Kubacka-Traczyk, and K. Gołaszewska-Malec, "Switchable double wavelength generating vertical external cavity surface-emitting laser," *Opt. Express* **22**(6), 6447–6452 (2014).
22. R. G. Bedford, M. Kolesik, J. L. A Chilla, and M. Reed, "Power-limiting mechanisms in VECSELs," *Proc. SPIE* **5814**, 199–208 (2005).